MOF-derived/zeolite hybrid catalyst for the production of light olefins from CO_2

Nuria Martín[+],*[a] Ander Portillo[+],[b] Ainara Ateka,[b] Francisco G. Cirujano,[c] Lide Oar-Arteta,[b] Andrés T. Aguayo,*[b] and Michiel Dusselier*[a]

In this contribution we propose an alternative catalytic system based on MOF derivatives and small pore zeolites for the selective conversion of CO_2 into light olefins, using the lowest metal loadings and highest GHSV reported in literature. The catalyst synthesis involves deriving In–Zr oxides from MOFs containing these metals in their structure, i.e. (Zr)UiO-67-bipy-In, via direct calcination in the presence of the zeolite, avoiding co-precipitation, washing and mixing steps. This effectively creates a truly bifunctional In–Zr zeolite catalyst, opposed to physical mixtures of two catalysts using different precursors. The good dispersion and low loadings of the MOF-derived In–Zr oxide supplemented with the strong acidity of chabazite-type zeolites allows to couple the activation of CO_2 with C–C coupling, obtaining space time yields of 0.1 mol of CO_2 converted to light olefins per gram of In per hour at 375 °C, under the GHSV conditions employed.

Introduction

Climate and pollution concerns, feedstock availability and geopolitical issues increase the need for alternative sustainable processes for the production of chemicals and fuels. In this context, the utilization of CO_2 as a feedstock (from carbon capture or concentrated point-sources) for making valuable compounds or intermediates, preferably containing more than one carbon, is a grand challenge of our time.[1–3] Among different strategies that aim to use CO_2 as a carbon feedstock, e.g. solar or electrochemical, classic thermo-catalytic methods certainly deserve their place.[4–5]

The hydrogenation of CO_2 to methanol (C1 product) presents such a route, provided one has a point source of CO_2, e.g. from industry or power plant flue gases (e.g. 10% pure), and sustainable hydrogen, e.g. from solar water splitting.[6] Reported systems for such CO_2 conversion, or the conversion of mixtures of CO_2 + syngas ($CO/CO_2/H_2$), often make use of a classic redox catalyst based on $Cu/ZnO/Al_2O_3$, with a crucial role for the metal/oxide interface.[7] Due to the stoichiometry of the gas-phase reaction and its exothermic nature ($CO_2 + 3H_2 \rightarrow CH_3OH + H_2O$, $\Delta H_{T=298K} = -49.3$ kJ/mol), both the increase in reaction pressure and decrease in reaction temperature, respectively, could favor CO_2 conversion and subsequent methanol formation. However the yield of methanol synthesized from CO_2 hydrogenation is kinetically limited at low temperatures (< 300 °C), requiring catalytic promotion.[8–10]

Among recent metal- and reducible oxide-based catalysts for the selective synthesis of methanol, In_2O_3 has been reported as a highly efficient catalytic system, avoiding side products such as CO from reverse water gas shift (RWGS), hydrocarbons, higher alcohols, etc. In the hydrogenation of CO_2 to methanol, this In_2O_3 catalyst achieves near 100% of selectivity and outstanding activity under (industrially) relevant conditions (T = 200–300 °C, P = 1.0–5.0 MPa, and gas hourly space velocities (GHSV = 16 000–48 000 h^{-1})).[11] These authors also showed that it is possible to increase the amount of active vacancies by adding CO to the gas feed or using the electronically interacting ZrO_2 as support for In_2O_3, resulting in a highly active and stable supported In_2O_3/ZrO_2 catalyst.

On top of novel methanol synthesis catalysts using CO_2, there has been an increased interest in the direct transformation of methanol into base petrochemicals, as methanol is a platform chemical that can be generated from non-petrol-derived feedstocks (e.g. coal, natural gas or biomass), through intermediate syngas.[12] Among those petrochemicals, light olefins (such as ethylene and propylene) are important building blocks in the chemical industry, with worldwide production in the range of 200 million tons per year (mainly from steam cracking today).[13] When methanol is activated in the presence of acid catalysts such as zeolites, it can be transformed into different hydrocarbons, depending on the porous structure of the molecular sieve in which the active proton site is located.[14]

In this sense, small pore zeotypes and zeolites (3.5–4 Å openings) with large cavities, e.g. CHA, AEI, DDR,[15–18] are able to convert methanol to light olefins (C2, C3 and some C4 alkene

[a] *Dr. N. Martín,[+] Prof. M. Dusselier*
Center for Sustainable Catalysis and Engineering (CSCE)
KU Leuven
Celestijnenlaan 200F
3001 Leuven (Belgium)
E-mail: nuria.martin@kuleuven.be
michiel.dusselier@kuleuven.be
[b] *A. Portillo,[+] Dr. A. Ateka, Dr. L. Oar-Arteta, Prof. A. T. Aguayo*
Department of Chemical Engineering
University of the Basque Country UPV/EHU
P.O. Box 644
48080 Bilbao (Spain)
E-mail: andrestomas.aguayo@ehu.eus
[c] *Dr. F. G. Cirujano*
Instituto de Ciencia Molecular (ICMol)
Universitat de Valencia
Catedrático José Beltrán Martínez n° 2
46980 Paterna, Valencia (Spain)
[+] *These authors contributed equally to this work*

building blocks for plastics). The large cavities allow the formation of the intermediate hydrocarbon pool and favor the diffusion of the produced light olefins out of the small pores, avoiding their further oligomerization and cracking.[19] Although still not a mature technology, the direct hydrogenation of the CO_2 to methanol combined with further C–C coupling into value-added products with two or more carbons, i.e. ethylene or propylene, is a very promising gas-to-liquid process.[20] This direct strategy allows for obtaining light olefins with a reduced number of steps and minimized chemical waste, while, most importantly, offering the prospect of fossil-fuel independent olefins production, hopefully with the net consumption of greenhouse gas CO_2.

An industrially viable heterogeneous catalyst is highly desired, however, this is challenging due to the inertness of CO_2, the combination of two sets of reaction conditions and the activation barriers of C–C coupling. On the one hand, the first step requires active metal or metal oxide species able to selectively reduce CO_2 into C1 oxygenate intermediates (e.g. methanol or CHO_x), avoiding undesired CO (from RWGS reaction) or the accumulation of methanol. On the other hand, the second transformation from the C1 oxygenate intermediates requires an acid catalyst with sufficient activity and selectivity during the C–C bond formations towards the desired light olefins. Note that in another route, i.e. CO_2 to syngas followed by Fisher-Tropsch chemistry, CO can be the desired intermediate, but not for the zeolite based C–C coupling.[21,22]

For the methanol route, the state-of-the-art so far has focused mainly on physically mixing two types of solid catalysts (redox, acid) in a single reactor vessel for both reductive and C–C coupling steps.[23–25] In this sense there are several reports combining the In–Zr oxides with oxygen vacancies (as methanol synthesis catalyst) and zeotype SAPO-34, based on its good performance in the methanol-to-olefins (MTO) process.[26–29] Such catalyst combination favors both the methanol generation on the surface of In_2O_3/ZrO_2, and the in situ conversion into light olefins, with high selectivities (80-90 % in the hydrocarbon fraction), shifting the equilibrium towards methanol in the first reaction and avoiding the undesired CH_4 fraction or even uncontrollable surface polymerization of CH_x (x = 1–3) on the metal surface.[26] However, the metal oxides obtained through co-precipitation methods require the use of stoichiometric amount of base, which presents a cost, safety and corrosion (handling-neutralization) concern. Moreover, the use of silico-alumino phospates as MTO catalysts often suffer from low stability and/or acid strength.[30]

In this work we propose, on the one hand, the use of aluminosilicate zeolites with the same CHA topology as zeotype SAPO-34, but with different acid strengths, and we compare their catalytic performances for the direct transformation of CO_2 into light olefins. On the other hand, we focus our attention on the use of In–Zr mixed metal organic frameworks (MOFs) as precursors of redox active and robust supported $(In–Zr)O_x$ nanoparticles uniformly distributed in (or on) the aluminosilicate phase (i.e. SSZ-13), after its thermal decomposition (see Figure 1). These MOFs could be cost-efficient since they can be potentially prepared from commercially available precursors

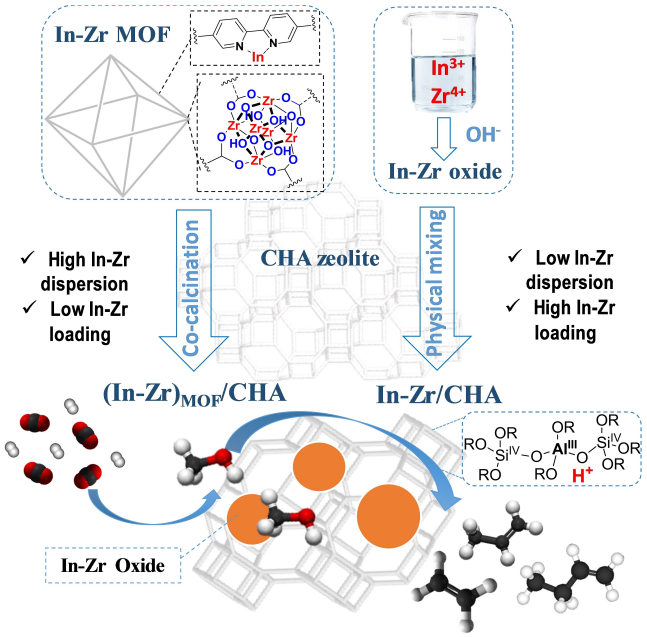

Figure 1. Different synthetic procedures for the obtention of In_2O_3/ZrO_2–CHA, either through physical mixture of the oxides and zeolite, or via co-calcination of the zeolite with (Zr)UiO-67-bipy-In MOF. The resulting hydrogenation/acid bifunctional catalysts are applied in the direct production of light olefins from CO_2.

using inexpensive, environmentally benign and scalable strategies, employing water as solvent, room temperature conditions or even rapid and clean mechanosynthesis.[31–33]

Furthermore, MOFs are an interesting alternative to the use of co-precipitated bulk metal oxides due to the fact that the metal (oxide precursor) sites are atomically dispersed in a metal organic crystalline framework and thus, it should produce less agglomerated and smaller nanoparticles after thermal decomposition of the linker in the close vicinity of the zeolite.[34–40] Recently, some of the authors here used this concept to create Zn and Cu oxide clusters on FAU zeolites for C–C and C–N couplings during the synthesis of fine chemical intermediates.[34] Moreover, different groups have employed MOFs or MOF derived catalysts in the hydrogenation of CO into hydrocarbons (Fischer-Tropsch) and hydrogenation of CO_2 into methanol or methane.[35–40] Here, we describe the possibility to use In–Zr-based MOFs as pre-catalysts in the presence of acid CHA zeolites, to yield truly bifunctional materials for the direct transformation of CO_2 into olefins (see $(In–Zr)_{MOF}$/CHA in Figure 1). This strategy allowed to decrease the In content and outperforms certain state-of-the art catalysts in terms of (CO_2-to-) olefins space time yield.

Results and Discussion

Structural and physico-chemical properties

First, different aluminosilicates as potential acid catalysts for the second C–C coupling step (MTO) were prepared.[41,42] Two zeolites with chabazite (CHA) structure and different acid contents (Si/Al = 15 and 30) were synthesized (see supporting information for synthesis details on all zeolites/zeotypes). A sample of benchmark SAPO-34, the commercial catalysts employed for this process, was also prepared.[43] Additionally the SSZ-39 small-pore zeolite with the AEI structure was prepared, given its good MTO performance, in order to compare possible effects of the cage structure (similar to CHA with small pores and large cavities) on the catalytic performance.[16,44] The microporous nature of the silicoaluminophosphate (SAPO-34) and zeolites was confirmed by N_2 physisorption, showing a higher porosity for the CHA zeolites (surface area 690 $m^2 g^{-1}$) with respect to the SAPO-34 (563 $m^2 g^{-1}$) or SSZ-39 (457 $m^2 g^{-1}$) samples, (see Figure S2 and Table S1 in the supporting information). The high external surface area of the chabazites (~150 $m^2 g^{-1}$) with respect to the SAPO-34 (~10 $m^2 g^{-1}$) indicates the nanosized nature of the zeolite crystals. This was confirmed by transmission electronic microscopy (TEM). The crystal sizes of the samples increase in the order: CHA < SAPO-34 < SSZ-39 (see Figure S6 and S7 in the supporting information). The different zeolites were mixed with In–Zr oxides (prepared via hydrothermal co-precipitation, see supporting information for details) in order to obtain the physically combined In–Zr/zeolites powder with a mass ratio 1:2 (zeolite/oxide). For that, In–Zr oxides and the corresponding zeolite were crushed together, pelletized and sieved (particle size of 0.25–0.5 mm). The In–Zr bulk oxide was characterized by an In content of 15.4 wt% (see Table S2 in the supporting information).

Secondly, we prepared a sample of (Zr)UiO-67-bipy-In MOF by solvothermal reaction between $ZrOCl_2 \cdot 8H_2O$, 2,2′-bipyridine-5,5′dicarboxylic acid and biphenyl-5,5′-dicarboxylic acid. The anchoring of In(III) to the bipyridine groups of the MOF is achieved by soaking the MOF in an ethanolic solution of In $(NO_3)_3H_2O$ (11 wt.% of In respect to the total MOF weight). The MOF structure and composition was confirmed by XRD, liquid ^{1}H-NMR and TGA (see Figures S3 and S4 in the supporting information). In order to obtain the MOF-derived In–Zr oxides, we have employed a recently reported methodology based on the use of metal-organic frameworks (MOFs) as precursors of metal oxide nanoparticles after thermal treatment at high temperature.[34–40] To the best of our knowledge, this MOF derived method has not been reported for In–Zr oxides in this particular catalytic application. Specifically, we have co-calcined the (Zr)UiO-67-bipy-In MOF (7 wt.% In) in the presence of the CHA_{30} zeolite with a MOF/zeolite mass ratio of 0.5/1. The resulting (In–Zr) oxide-zeolite hybrid material should have a mass ratio of zeolite:oxide of 7:1, based on the metal content of the MOF and stoichiometric oxide formation of In^{III} and Zr^{IV} after co-calcination. The detailed synthesis and characterization of the MOF is described in section 1 of the supporting information). Importantly, the In content in the final composite was only 2.3 wt% (see the ICP analysis in table S2 of the supporting information).

For both co-calcined MOF-zeolite and co-precipitated oxide-zeolites, the PXRD patterns of the final In–Zr/zeolites mixtures show the preservation of the zeolite crystalline structure, and the presence of the In–Zr oxide phase reflections at $2\theta = 30$, 35 and 50 degrees (see Figure 2 a). NH_3-Temperature-Programmed Desorption (NH_3-TPD) indicates a higher total amount of acid sites in the case of the physically-mixed In–Zr/CHA sample (136 mmol NH_3/g) with In_2O_3/ZrO_2, with respect to the $(In–Zr)_{MOF}$/CHA (101 mmol NH_3/g) with the MOF derived In_2O_3/ZrO_2 prepared by co-precipitation in the presence of the zeolite (see Figure 2b). The incorporation of MOF-derived In_2O_3/ZrO_2 in close contact with the zeolite slightly decreases the number of acid sites and affects their strength distribution as well, as described for CuO/ZnO on FAU zeolite.[34] Finally, the TEM images indicate a better dispersion of the In_2O_3/ZrO_2 in the $(In–Zr)_{MOF}$/CHA with respect to the In–Zr/CHA physical mixture. For the latter, the higher loading of In–Zr, in accord with the ICP results, is clear from TEM as well (see Table S2 in the supporting information).

Catalytic properties

The performance of the different samples for the hydrogenation of CO_2 at different temperatures was studied. The tests were conducted with a H_2/CO_2 feed gas ratio of 3/1. For all samples, CO_2 starts to be converted at temperatures higher than 350 °C, with almost no conversion at lower temperatures, under the reaction conditions employed (see Figure 3a). In our hands, the benchmark physically mixed In–Zr/SAPO-34 sample, shows an In-based reaction rate (amount of CO_2 converted per bulk indium weight and time) that increases in parallel with the reaction temperature (from $1 \cdot 10^{-4}$ $mol_{CO2}\, g_{In}^{-1}\, s^{-1}$ at 375 °C to $9 \cdot 10^{-4}$ $mol_{CO2}\, g_{In}^{-1}\, s^{-1}$ at 450 °C), as shown in Figure 3a. The In–Zr oxide mixed with the CHA_{30} zeolite with high Si/Al ratio of 30, shows an In-based conversion rate higher to that of the CHA_{15} with Si/Al ratio of 15 ($1.3 \cdot 10^{-4}$ *vs.* $7.9 \cdot 10^{-5}$ $mol_{CO2}\, g_{In}^{-1}\, s^{-1}$, respectively) at 375 °C. This either highlights a remarkable contribution of strong acid sites (for the same type and content of mixed In–Zr oxides in both zeolite samples) to the hydrogenation of CO_2 or, alternatively, that the zeolite-based differences in MTO chemistry affect the equilibrium or conversion rate of the first step. The latter seems more plausible, i.e. the CHA with a higher Si/Al ratio induces a higher CO_2 conversion rate, pointing to the fact that the strong acidity favours a quicker conversion of the methanol produced (pulling it away from its CO_2 hydrogenation equilibrium), into light olefins (with respect to other hydrocarbons), rather than accumulating oxygenated intermediates. The latter occurs with SAPO-34, as we will further discuss when analysing product distributions.

Given the good performance of the In–Zr/CHA_{30} sample, we decide to investigate routes to decrease the In–Zr loading, while maintaining or improving the good catalytic performance of using a zeolite (instead of a SAPO). The MOF-derived sample

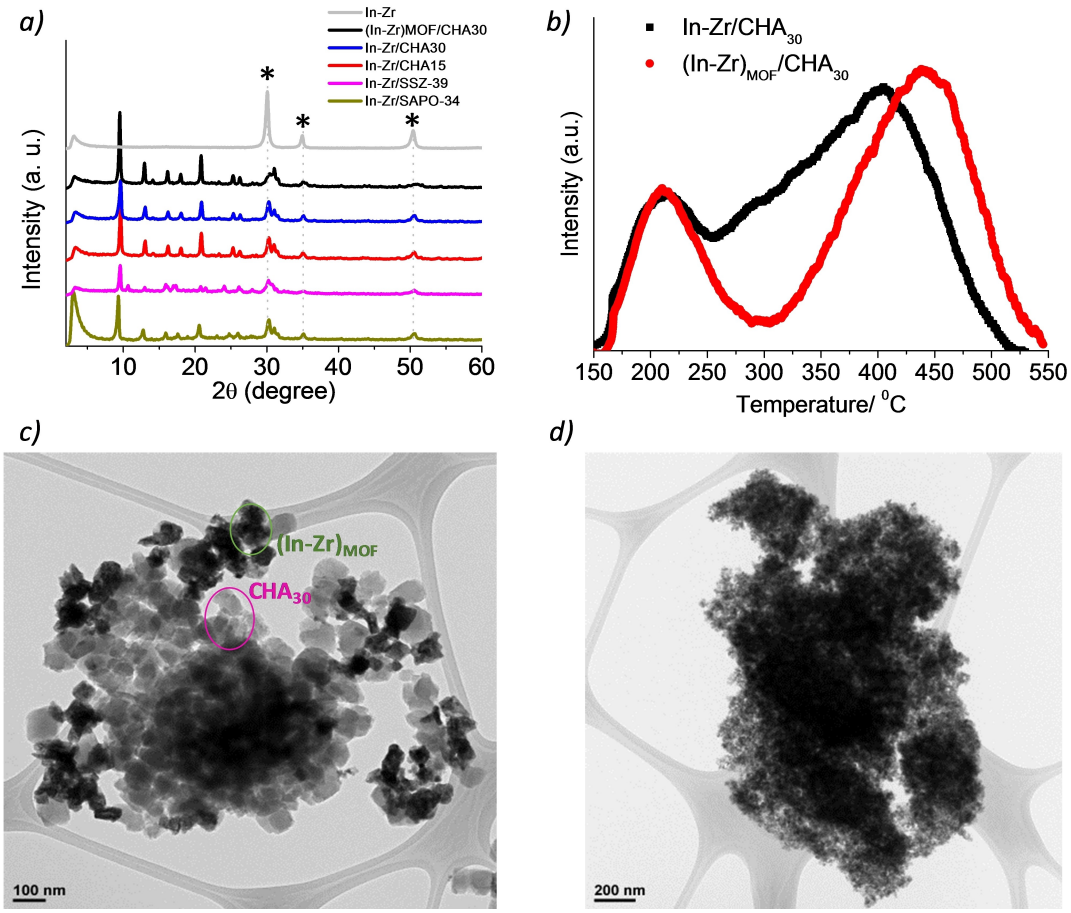

Figure 2. (a) PXRD patterns of the catalyst samples employed in this work. (b) NH_3-TPD of the $(In–Zr)_{MOF}$/CHA (red) and In–Zr/CHA (black) catalysts. (c) TEM image of $(In–Zr)_{MOF}$/CHA. (d) TEM image of In–Zr/CHA.

described previously fulfils this requirements, and, in fact, the $(In–Zr)_{MOF}/CHA_{30}$ exhibit the highest CO_2 conversion values per g_{In} at temperatures higher than 425 °C ($1\cdot10^{-3}$ $mol_{CO2}\,g_{In}^{-1}\,s^{-1}$).At lower temperatures comparable conversions to that of In–Zr/CHA_{30} are observed (see Figure 3a). The In-based reaction rate per g of indium (as metal, but present in oxide form) obtained with the sample of In–Zr/SAPO-34 prepared in this work, is different than the previously reported ones ($2\cdot10^{-4}$ *vs.* $1\cdot10^{-4}$ $mol_{CO2}\,g_{In}^{-1}\,s^{-1}$ at 400 °C, 3 MPa, $H_2/CO_2 = 3/1$), probably due to the high GHSV employed here, 78300 *vs.* 9000 ml $g_{cat}^{-1}\,h^{-1}$ (expressed as the space time velocity in ml·$g_{cat}^{-1}\,h^{-1}$).[23] A high space velocity is industrially interesting if the conversions rate can remain high, since it allows minimizing the amount of catalyst or contact time, which results in a faster and cheaper catalytic system.

However, for temperatures higher than 400 °C, the major part of the CO_2 is hydrogenated into CO, through the favoured (endothermic) reverse water gas shift reaction (see Figure 3b and c).

The selectivity of hydrocarbons with respect to that of CO at the edge temperature of 375 °C is 10% higher for the MOF-based hybrid sample with respect to the co-precipitated oxides mixed with CHA, at comparable CO_2 conversion rate (~$1\cdot10^{-4}$ $mol_{CO2}\,g_{In}^{-1}\,s^{-1}$). This indicates that the MOF derived sample promotes to a higher extent the hydrogenation (at the well-dispersed In–Zr MOF-derived oxides) of CO_2 into CH_xO intermediates that further migrate to the nearby strong Brønsted acid sites of the CHA, resulting in the corresponding hydrocarbons (see Figure 3c). The CH_xO species likely run through methanol synthesis and with transformation of the methanol into light olefins. This is corroborated by the product slate of the In–Zr/SAPO-34 where the oxide part of the physically mixed catalyst generated methanol with 13% selectivity in the hydrocarbon fraction at 375 °C (see blue bar in Figure 3d).

In the case of In–Zr/SAPO-34, the olefin selectivity at 375 °C in the hydrocarbon phase (see Figure 3d) is significantly lower with respect to the $(In–Zr)_{MOF}/CHA_{30}$ (69 *vs.* 87%), highlighting the importance of the strong acidity in the conversion of the methanol produced into light olefins and avoiding the accumulation of oxygenated intermediates. Zeolites allow performing MTO at slightly lower temperature than SAPO zeotypes. The co-precipitated $In–Zr/CHA_{30}$ selectivity is lower than the MOF derived one (76%), although still higher than samples with a less well performing acid component (see Figure 3d), e.g. $In–Zr/CHA_{15}$ (45%), In–Zr/SSZ-39 (49%) and In–Zr/SAPO-34

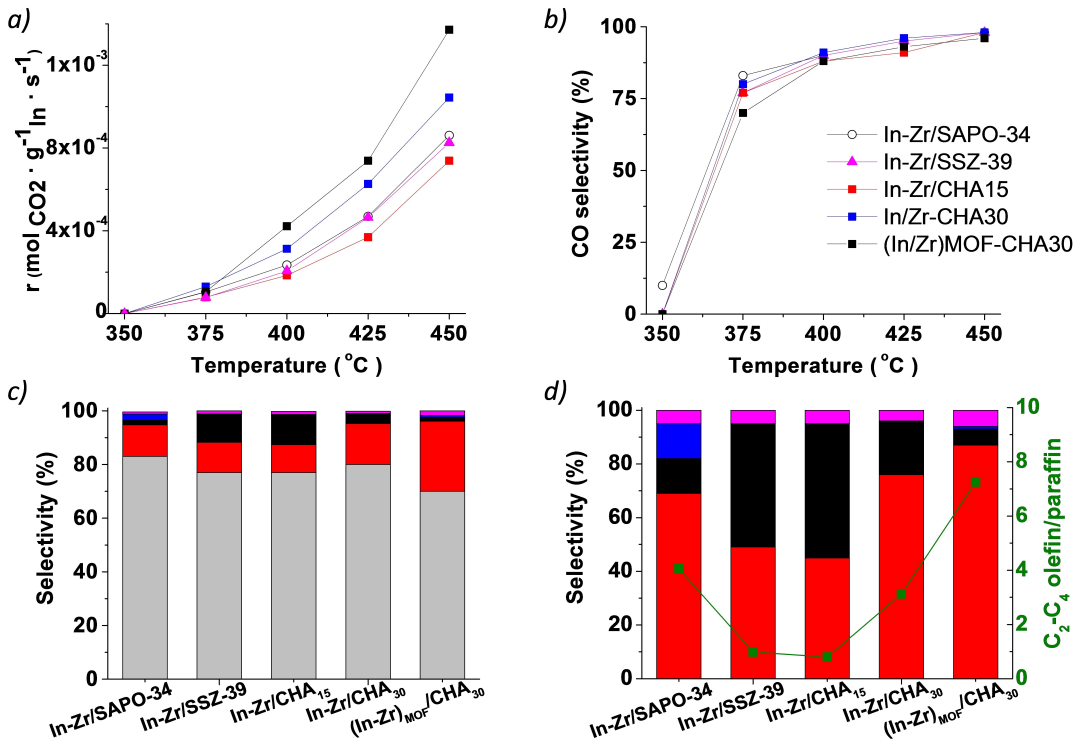

Figure 3. Conversion rate (r) of CO_2 per In weight, obtained from the equation $r = Flow_{CO2} \cdot \frac{\frac{Conv.CO_2}{100}}{22.4\ g_{In}}$ (a) and selectivity to CO (b) at different temperatures for the series of catalysts. Selectivity of products: olefins (red), paraffins (black), methane (magenta) and oxygenates (blue); with respect to the selectivity of CO (grey) at 375 °C (c). The product distribution without considering CO is shown in part (d), together with the C_2–C_4 olefin/paraffin ratio (see green dots), both at T = 375 °C.

(69 %) at 375 °C, for comparable CO_2 rate (~ $1 \cdot 10^{-4}$ $mol_{CO2}\, g_{In}^{-1}\, s^{-1}$). The lower selectivity obtained with In–Zr/CHA_{15} containing a high amount of Brønsted acid sites originates partially from its higher CO selectivity, but may also be due to the favoured oligomerisation and cracking of the lower olefins in the more aluminous zeolite, with generation of coke. In fact the lower Si/Al ratio results in SSZ-13 samples with more than one Al per cavity (i.e. Al pairs) which is reported to be correlated with both coke species formation and rapid deactivation.[45–47] Moreover, the reduced Brønsted acidity of CHA(Si/Al = 30) also inhibits H-transfer reactions (and consequently oligomerization) giving additional light olefins at the expense of longer chain hydrocarbons, thus increasing the selectivity towards olefins with respect to CHA(Si/Al = 15), as has been recently proposed for ZSM-5 (see Figure S11 for the analysis of coke formation on the used catalyst, c.a. 4 wt.%).[48] Beside coke formation and blocking of acid sites in the zeolite, indium (III) cation migration during the reaction may exchange with the zeolite protons, further decreasing the acidity (see Figure S12). A similar catalyst behaviour is observed for the In–Zr/SSZ-39 sample with similar acidity (Si/Al ratio). The olefin/paraffin ratios plotted in Figure 3d corroborate this interpretation (see C2-C4 olefin/paraffin in green). In general, for the best samples, i.e. $(In–Zr)_{MOF}/CHA_{30}$ and In–Zr/CHA_{30}, it can be hypothesized that the small size of the CHA zeolite crystals (estimated at 50–100 nm by TEM analysis, see Figure 2c and Figure S6) favours the fast transformation of CH_xO intermediates into hydrocarbons due to the favoured diffusion (of the CH_xO intermediates generated at the In–Zr oxide particles) to the acid sites in the nanocrystals. This partially suppresses the undesired RWGS side-reaction to CO and possibly avoids excessive olefin oligomerisation and cracking further impeded by relatively low Al-contents. Similar results have been recently reported for nanosized CHA or SAPO-34 in MTO, and also for different In–Zr/SAPO-34 catalysts in CO_2 conversion.[27,28] There, small crystal sizes are indeed deemed interesting to shorten the diffusion path of the methanol intermediates and enhance the selectivity of $C_2^{=}$–$C_4^{=}$.[30]

As pointed out earlier, the C_2–C_4 olefin/paraffin (o/p) ratios significantly augments with the Si/Al ratio (from 15 to 30), and with the use of MOF-derived In–Zr oxides instead of co-precipitated ones (see Figure 3d). The latter is intriguing and indicates favouring the generation of olefins over paraffins, by avoiding (or reducing) hydrogen transfer reactions at the acid sites present in the modified CHA versus when using the standard co-precipitated approach. This could be related to the slightly altered and lower amount of acid sites in the MOF-derived sample, as seen from NH_3-TPD in Figure 2b. Based on the reaction pathway of CO_2 hydrogenation over oxide/zeolite mixed catalysts, CO_2 firstly hydrogenates to the methanol intermediate on the metal oxide phase, and then the intermediate transfers to the acid sites of the zeolite for C–C

coupling to generate hydrocarbons. The proximity of these two types of active sites can play an important role in giving a high selectivity for desired light olefins (mainly ethylene and propylene, as shown in Figure S9c). In the case of the well-dispersed MOF derived hybrid $(In–Zr)_{MOF}/CHA_{30}$, the distances between the In–Zr sites and the acid sites are likely shorter (tentative in Figure 2c), favouring the transformation of methanol or CO intermediates into the desired hydrocarbons.

In order to put our work in context, the values of space-time yield obtained with the samples prepared in this work (entries 8–12 in Table S5) were compared with those reported in literature (entries 1–7 in Table S5). In general, it is clear from these two groups of results that the use of a higher GHSV results in a higher amount of olefins produced per hour and gram of catalyst ($STY_{olefins}$). Despite the good selectivities to olefins in most cases, the CO_2 conversions are below the reported values obtained for lower GHSV, likely the effect of the shorter contact times in our case. The best performing catalyst is the one containing SSZ-13 (CHA, Si/Al = 30), with a productivity per gram of catalyst one order of magnitude higher (entry 10 in Table S5) than state-of-the-art In/Zr containing catalysts. Both the MOF- derived In–Zr (entry 11) and the co-precipitated In–Zr physical mixed one (entry 10) with the CHA_{30} zeolite show the best performances on an In–Zr oxide basis, with the highest productivity found for the MOF-derived one (see Figure 4a). This material allows to decrease the In–Zr content, resulting in a more economic catalyst for the process of CO_2 hydrogenation, maintaining one of the highest selectivities to olefins (26% when including CO, see entry 11), reported to date. This high selectivity, together with the better catalytic activity results in an outperformance of the rate of olefins produced per In weight (see Figure 4b). Indeed, the STYs on a bulk In basis is 1.4 times higher in the case of the MOF derived hybrid catalyst (98 $mmol_{olefins}\,g_{In}^{-1}\,h^{-1}$), with respect to the co-precipitated InZr/CHA_{30} mixture (72 $mmol_{olefins}\,g_{In}^{-1}\,h^{-1}$) and more than two times higher than state-of-the-art In–Zr/SAPO-34 physical mixtures, in our setup (43 $mmol_{olefins}\,g_{In}^{-1}\,h^{-1}$). Both MOF derived hybrid and co-precipitated catalysts show a decent stability under the different reaction temperatures, as indicated by the stable conversion values over time (see Figures S8 and S9).

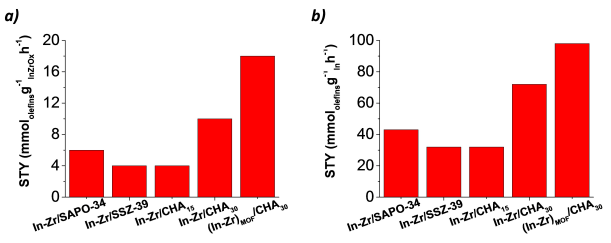

Figure 4. Production rate (Space Time Yields) for C2–C4 olefins per In–Zr oxide weight (a) or In weight (b) at 375 °C with the samples prepared in this work. A feed of CO_2 and H_2 with a flow of 60 ml min^{-1} ($H_2/CO_2 = 3/1$) was employed at 30 bar, using 46 mg of catalysts. Note that the STYs are calculated on a mmol CO_2-to-olefins basis.

Conclusion

Herein, we have reported for the first time the use of small pore zeolites, opposed to zeotypes, as acid catalysts in the preparation of physically mixed In–Zr oxide/zeolite cocktail catalysts for the upgrading of CO_2 into light olefins. This demonstrated the importance of acid strength and controlling the acidity by varying the Si/Al ratio for the catalytic CO_2-to-methanol-to-olefins cascade. Moreover, this contribution has shown that it is possible to decrease the number of redox active sites needed (e.g. on an Indium basis, which is a costly metal) for the hydrogenation of CO_2 into light olefins via a MOF-derived approach in order to prepare novel bifunctional hydrogenation-acid tandem catalysts.

This synthesis method allows to prepare In–Zr oxides derived from MOFs, containing these metals in its structure, via direct co-calcination in the presence of the zeolite, avoiding co-precipitation and washing and mixing steps. In this manner, a truly In–Zr/zeolite bifunctional catalyst can be created, opposed to physical mixtures of two catalysts using different precursors. A comparison of olefins space-time yields was made, and in our conditions of high space velocity, the productivity of the MOF-derived catalytic system seems among the highest reported, with 18 $mmol_{olefins}\,g_{InZrOx}^{-1}\,h^{-1}$ and 98 $mmol_{olefins}\,g_{In}^{-1}\,h^{-1}$. The MOF-derived In–Zr/CHA severely outperforms benchmark silicoaluminophosphates physically mixed with co-precipitated In–Zr oxides. Overall, absolute olefin yields (here and in the art) remain low in this cascade, highlighting one of the major challenges in direct CO_2-to-olefins catalysis still ahead.

Experimental Section

Synthesis of the catalysts

Obtention of In_2O_3/ZrO_2 by coprecipitation method:[26] On the one hand, the coprecipitation of indium and zirconium oxides was carried out starting from 3.9 g of indium nitrate and 17.6 g zirconium nitrate dissolved in a mixture of 50 mL of deionized water and 150 mL of ethanol. On the other hand, a solution containing 34 mL of ammonia hydroxide (NH_4OH 28–30 wt% in H_2O, Sigma Aldrich) in 110 mL of ethanol was added dropwise over the previous mixture. The product was aged at 80 °C for 30 min and then filtered, washed with deionized water, dried overnight at 60 °C and calcined in air at 500 °C for 5 h.[23]

Synthesis of SAPO-34:[26] The silicoaluminophosphate SAPO-34 (CHA) was prepared mixing 1,9 g of aluminium hydroxide ($Al(OH)_3$, ≥64% Al_2O_3, Sigma-Aldrich) with 2.1 g of phosphoric acid (H_3PO_4, 85 wt%. Sigma Aldrich) in 2.8 g of deionized water (18.2 MΩ cm). Finally, 8.5 g of tetraethylammonium hydroxide (TEAOH, 35 wt%. Sigma Aldrich) and 0.7 g of colloidal suspension of silica in water (40 wt %, LUDOX-AS, Sigma–Aldrich) were introduced in the gel and the mixture was stirred for 30 min. The resulting get was transferred to an autoclave with a Teflon liner (Parr Instruments), and heated at 160 °C during 5 days.[23] The molar composition of the final gel was:

$$0.44\,SiO_2 : Al_2O_3 : P_2O_5 : 1.6\ TEAOH : 40\,H_2O$$

The final products were centrifuged, washed with abundant water and dried at 100 °C. All samples were calcined in air with a heating ramp of 3 °C/min to 580 °C for 5 hours to remove organic template.

Synthesis of CHA zeolites:[43] The synthesis of SSZ-13 zeolites (CHA) was achieved using *N,N,N*-**trimethyladamantammonium** as organic structure directing agent. The required amounts of a 25 wt% aqueous solution of *N,N,N*-**trimethyladamantammonium** (TMAdaOH, 25 wt% Sachem) and a 20 wt% aqueous solution of sodium hydroxide (Sigma–Aldrich) were mixed. Then the required amounts of alumina (Al_2O_3, Sigma Aldrich) and a colloidal suspension of silica in water (40 wt% LUDOX-AS, Sigma-Aldrich) were added and the resultant mixture was stirred for the time required to evaporate the excess of water until achieving the desired gel concentration. The final molar batch compositions were:

$$CHA_{15}: \ SiO_2/0.033Al_2O_3/0.4TMAdaOH/0.2NaOH/15H_2O$$

$$CHA_{30}: \ SiO_2/0.017Al_2O_3//0.4TMAdaOH/0.2NaOH/15H_2O$$

The homogeneous gel was transferred to a 40 mL Teflon lined stainless steel autoclave (Parr Instruments) and heated at 160 °C in an oven for 10 days. The final products were centrifuged, washed with abundant water and dried at 100 °C. All samples were calcined in air with a heating ramp of 3 °C/min to 580 °C for 5 hours to remove organic template. The sodium-containing materials were mixed with a 1 M aqueous solution of ammonium nitrate and the mixture was stirred at 80 °C for 2 h. The solid product was filtered, washed with abundant water, and dried at 100 °C. Finally, the solid was calcined in air at 500 °C for 4 h.

Synthesis of SSZ-39 zeolite:[16] The synthesis of SSZ-39 zeolite (AEI) was achieved in the presence of *N,N*-dimethyl-3,5-dimethylpiperidinium as organic structure directing agent. *N,N*-dimethyl-3,5-dimethylpiperidinium (DMP) cation was synthesized starting from 15 g of 3,5-dimethylpiperidine ($C_7H_{15}N$, Sigma Aldrich, $\geq$ 99 %, cis-trans mixture) dissolved in 140 mL of methanol (CH_3OH, Acros Organics, 99.99 %) in presence of 20 g of potassium carbonate ($KHCO_3$, Sigma Aldrich, 99.7 %). 55 g of methyl iodide (CH_3I, Sigma Aldrich, 99.9 %) were added dropwise to the previous solution. Then the resultant mixture was maintained under stirring for 6 days. After this time, MeOH was partially removed under vacuum, and the iodide salt was precipitated by addition of diethyl ether. For preparing the corresponding hydroxide form, the iodide salt was dissolved in water in the presence of a commercially available hydroxide ion exchange resin, and it was maintained under stirring overnight. The final solution was filtered obtaining an aqueous solution containing the *N,N*-dimethyl-3,5-dimethylpiperidinium hydroxide. For the *SSZ-39 synthesis*, 3.4 g of aqueous solution of DMP (35 %) and 1.5 g of 20 wt% aqueous solution of sodium hydroxide (Sigma–Aldrich) were mixed. Then 6.7 g of deionized water and 2 g of commercial Faujasite (FAU, CBV-720, Zeolyst) were added to the previous solution achieving the final gel with the following molar composition:SSZ-39:

$$SiO_2/0.033Al_2O_3/0.2 \ DMP \ /0.2NaOH/15H_2O$$

The homogeneous gel was transferred to a 20 mL Teflon lined stainless steel autoclave (Parr Instruments) and heated at 140 °C in an oven for 10 days. The final product was centrifuged, washed with abundant water and dried at 100 °C. The samples was calcined in air with a heating ramp of 3 °C/min to 580 °C for 5 hours to remove organic template. The sodium-containing material was mixed with a 1 M aqueous solution of ammonium nitrate and the mixture was stirred at 80 °C for 2 h. The solid product was filtered, washed with abundant water, and dried at 100 °C. Finally, the solid was calcined in air at 500 °C for 4 h.

Preparation of physical mixtures: The different zeolites were physically mixed with In–Zr oxides in order to obtain the bifunctional catalyst with a mass ratio 2/1. For that In–Zr oxides and the corresponding zeolite were together crushed, pelletized and sieved (particle size of 0.25–0.5 mm).

Synthesis and characterization of the novel In-Zr MOFs: *The* solvothermal synthesis of UiO-67 MOFs starts by mixing 400 mg $ZrOCl_2 \cdot 8H_2O$, 300 mg Bipy (2,2′-bipyridine-5,5′dicarboxylic acid) and 100 mg BPDC (biphenyl-5,5′-dicarboxylic acid) in 10 mL DMF and 1 mL HAc in a 100 mL pyrex Schott bottle. This solution is put in an ultrasound bath for 10 min, until all reactants are fully dissolved. After one day in a conventional synthesis oven at 120 °C, a gel phase has formed. The final crystal form is reached by utilizing the Büchner filtration method accompanied by consecutively washing with copious amounts of DMF and EtOH. The anchoring of In(III) to the bipy groups of the MOF is achieved through the following procedure: 300 mg of $In(NO_3)_3H_2O$ were dissolved in 7 ml of EtOH and added to 1 g of $Zr_6O_4(OH)_4[BPDC]_{2.28}[Bipy]_{3.72}$ (~ 11 wt.% In respect to the MOF). After stirring at 30 °C overnight, the solid was recover by centrifugation and washed three times with fresh EtOH. The sample was dried at 60 °C overnight under vacuum.

Synthesis of the novel In-Zr MOF derived oxides in zeolites: Briefly, 1 g of zeolite (e.g. CHA) was physically mixed with 0.5 g of UiO-67-bipy-In (containing a 7 %wt. of In) in a moulter, and subsequently calcined at 580 °C during 5 h. The amount of In in the final mixture was 2.5 %wt.

Characterization of the catalysts

X-ray powder diffraction (XRD) patterns were acquired on a STOE stadi MP using Cu K-α radiation. Nitrogen-sorption (N_2-sorption) was measured with a Micromeritics TriStar 3000 instrument at 77 K. Samples were pretreated overnight under a N_2 flow at 573 K before the measurements. The surface area was calculated by the BET method. The t-plot method was used to determine the micropore volume. The amount of In and Zr as well as the Si/Al ratio in the solid catalysts was determined by ICP Optical Emission Spectroscopy (Varian 720-ES). Ammonia temperature-programmed desorption (NH_3-TPD) was measured in a flow apparatus with a mass spectrometer for the desorbed gas (NH_3). After pretreatment of the samples (100 mg) in helium flow at 673 K for 2 h, adsorption of NH_3 was conducted at 473 K for 0.5 h. Afterward, the sample was flushed by helium for 0.5 h at 473 K. NH_3-TPD profiles were obtained by heating the sample in a helium flow to 823 K with a ramping rate of 10 K min^{-1}. Transmission Electron Microscopy (TEM) was performed using a 200 kV JEOL JEM-2010 microscope. The study of the reducibility of the metallic functions has been performed by temperature-programmed reduction (TPR) using a Micromeritics Autochem 2920 equipment. In this analysis, a sample of approximately 100 mg was loaded into a ''U'' quartz reactor, and subjected to the following analysis steps: (i) sweeping with He to eliminate possible impurities at 200 °C for 2 h; (ii) stabilization of the sample at room temperature (15 min) in a diluted H_2 stream (10 % of H_2 diluted in Ar); (iii) heating of the sample with a temperature ramp of 2 °C min^{-1} up to 700 °C. The H_2 consumption was detected by a thermal conductivity detector (TCD).

Catalytic tests

The automated reaction equipment (PID Eng. & Tech. Micro-activity Reference) is provided with a high-pressure fixed-bed isothermal reactor system. The reactor is made of 316 stainless steel, has an internal diameter of 9 mm and 10 cm of effective length and is located inside a stainless steel covered ceramic chamber heated by an electric resistance. The equipment can operate up to 700 °C and 100 atm with a catalyst mass up to 5 g. In order to ensure the isothermality of the bed (avoiding hot spots) and attaining a sufficient bed height under low space time conditions, the catalyst is mixed with an inert (SiC of 0.035 mm average particle size). Reaction products (diluted in a He stream of 25 cm^3 min^{-1}) are continuously analyzed (online) in a Varian CP-4900 gas microchromatograph provided with three analytical modules, with the following columns: (i) Porapak Q (PPQ, 10 m × 20 μm), for the quantification of CO_2, methane, methanol, DME, water and C1-C4 hydrocarbons; (ii) a molecular sieve (MS-5, 10 m × 12 μm), for the separation of H_2, CO, O_2 and N_2; (iii) 5CB (CPSiL, 8 m × 2 μm), for the quantification of the C5–C10 hydrocarbons fraction (if any, formed in insignificant quantity). A feed of CO_2 and H_2 with a flow of 60 ml min^{-1} ($H_2/CO_2 = 3/1$) was employed at 30 bar, using 46 mg of catalysts in each test and operating at different temperatures. The conversion was calculated based on the amount of CO_2 feed that has been converted into products: CO_2 conversion $= (CO_2^{inlet}\text{-}CO_2^{outlet})/CO_2^{inlet}$. For the quantification of the selectivity of *i* product (i = CO, olefins, paraffins, methane and oxygenates), the following ratio has been established: $S_i = F_i/\Sigma F_i$, where F_i is the molar flow rate of the i compound in the product stream.

Acknowledgements

N.M. acknowledge the European Commission-Horizon 2020 for funding through Marie Sklodowska Curie Individual Fellowship under the grant agreement: 792943 (ZEOCO2). The Ministry of Economy and Competitiveness of the Spanish Government is acknowledged for funding (CTQ2016-77812-R). F.G.C. acknowledge that the project leading to these results has received funding from "la Caixa" Foundation (ID 100010434), under agreement < LCF/BQ/PI19/11690011 >. SACHEM is thanked for providing the TMAdaOH organic structure directing agent for SSZ-13. M.D. acknowledges KU Leuven Internal Funds and BOF. We are grateful to Cristina Almansa for performing the TEM analysis of the samples at the research technical services of the University of Alicante in Spain.

Conflict of Interest

The authors declare no conflict of interest.

Keywords: CO_2 hydrogenation · zeolites · MOFs · olefins

[1] S. Roy, A. Cherevotan, S. C. Peter, *ACS Energy Lett.* **2018**, *3*, 1938–1966.
[2] J. Artz, T. E. Müller, K. Thenert, J. Kleinekorte, R. Meys, A. Sternberg, A. Bardow, W. Leitner, *Chem. Rev.* **2018**, *118*, 434–504.
[3] J. A. Martens, A. Bogaerts, N. De Kimpe, P. A. Jacobs, G. B. Marin, K. Rabaey, M. Saeys, S. Verhelst, *ChemSusChem.* **2017**, *10*, 1039–1055.
[4] B. M. Tackett, E. Gomez, J. G. Chen, *Nat. Can.* **2019**, *2*, 381–386.
[5] E. V. Kondratenko, G. Mul, J. Baltrusaitis, G. O. Larrazábalc, J. Pérez-Ramírez, *Energy Environ. Sci.* **2013**, *6*, 3112–3135.
[6] W. Zhou, K. Cheng, J. Kang, C. Zhou, V. Subramanian, Q. Zhang, Y. Wang, *Chem. Soc. Rev.* **2019**, *48*, 3193–3228.
[7] A. Bansode, A. Urakawa, *J. Catal.* **2014**, *309*, 66–70.
[8] J. Chunmiao, G. Jiajian, Y. Dai, J. Zhang, Y. Yang, *J. Energy Chem.* **2016**, *25*, 1027–1037.
[9] M. Ronda-Lloret, G. Rothenberg, N. R. Shiju, *ChemSusChem* **2019**, *12*, 3896–3914.
[10] Z. Ma, M. D. Porosoff, *ACS Catal.*, **2019**, *9*, 2639–2656.
[11] O. Martin, A. J. Martín, C. Mondelli, S. Mitchell, T. F. Segawa, R. Hauert, C. Drouilly, D. Curulla-Ferré, J. Pérez-Ramírez, *Angew. Chem. Int. Ed.* **2016**, *55*, 6261–6265.
[12] G A. Olah, A. Goeppert, G. K. S. Prakash, *Beyond Oil and Gas: The Methanol Economy*, 2nd. Ed., **2009**, Wiley VCH Verlag GmbH & Co. KGaA.
[13] H. M. Torres Galvis, K. P. de Jong, *ACS Catal.* 3 (2013) 2130–2149.
[14] P. Tian, Y. Wei, M. Ye, Z. Liu . *ACS Catal.*53 (2015) 1922–1938.
[15] U. Olsbye, S. Svelle, M. Bjørgen, P. Beato, T. V. Janssens, F. Joensen, S. Bordiga, K. P. Lillerud, *Angew. Chem. Int. Ed.* **2012**, *51*, 5810–5831.
[16] N. Martín, Z. Li, J. Martínez-Triguero, J. Yu, M. Moliner, A. Corma, *Chem. Commun.*, **2016**, *52*, 6072–6075.
[17] I. Yarulina, J. Goetze, C. Gücüyener, L. van Thiel, A. Dikhtiarenko, J. Ruiz-Martinez, B. M. Weckhuysen, J. Gascon, F. Kapteijn, *Catal. Sci. Technol.* **2016**, *6*, 2663–2678.
[18] M. Dusselier, M. E. Davis, *Chem. Rev.* **2018**, *118*, 5265–5329.
[19] V. Van Speybroeck, K. De Wispelaere, J. Van der Mynsbrugge, M. Vandichel, K. Hemelsoet, M. Waroquier, *Chem. Soc. Rev.* **2014**, *43*, 7326–7357.
[20] W. Li, H. Wang, X. Jiang, J. Zhu, Z. Liu, X. Guo, C. Song, *RSC Adv.* **2018**, *8*, 7651–7669.
[21] A. Dokania, A. Ramirez, A. Bavykina, J. Gascon, *ACS Energy Lett.* **2019**, *4*, 167–176.
[22] A. Ramirez, A. Dutta Chowdhury, A. Dokania, P. Cnudde, M. Caglayan, I. Yarulina, E. Abou-Hamad, L. Gevers, S. Ould-Chikh, K. De Wispelaere, V. van Speybroeck, J. Gascon, *ACS Catal.*, **2019**, *9*, 6320–6334.
[23] P. Gao, S. Li, X. Bu, S. Dang, Z. Liu, H. Wang, L. Zhong, M. Qiu, C. Yang, J. Cai, W. Wei, *Nat.Chem.* **2017**, *9*, 1019–1024.
[24] J. Wei, Q. Ge, R. Yao, Z. Wen, C. Fang, L. Guo, H. Xu, *Nat. Commun.* **2017**, *8*, 15174–15182.
[25] J. Gao, C. Jia, B. Liu, *Catal. Sci.* Technol. **2017**, *7*, 5602–5607.
[26] P. Gao, S. Dang, S. Li, X. Bu, Z. Liu, M. Qiu, C. Yang, H. Wang, L. Zhong, Y. Han, Q. Liu, W. Wei, Y. Sun, *ACS Catal.* **2018**, *8*, 571–578.
[27] S. Dang, S. Li, C. Yang, X. Chen, X. Li, L. Zhong, P. Gao, Y. Sun, *ChemSusChem.* **2019**, *12*, 3582–3591.
[28] S. Dang, P. Gao, Z. Liu, X. Chen, C. Yang, H. Wang, L. Zhong, S. Li, Y. Sun, *J. Catal.* **2018**, *364*, 382–393.
[29] J. Chen, X. Wang, D. Wu, J. Zhang, Q. Ma, X. Gao, X. Lai, H. Xia, S. Fan, T.-S. Zhao, *Fuel* **2019**, *239*, 44–52.
[30] F. Bleken, M. Bjørgen, L. Palumbo, S. Bordiga, S. Svelle, K. P. Lillerud, U. Olsbye, *Top. Catal.* **2009**, *52*, 218–228.
[31] Z. Chen, X. Wang, H. Noh, G. Ayoub, G. W. Peterson, C. T. Buru, T. Islamoglu, O. K. Farha, *CrystEngComm*, **2019**, *21*, 2409–2415.
[32] B. Karadeniz, A. J. Howarth, T. Stolar, T. Islamoglu, I. Dejanovic, M. Tireli, M. C. Wasson, S. Y. Moon, O. K. Farha, K. Uzarevic, *ACS Sust. Chem. Eng.* **2018**, *6*, 15841–15849.
[33] A. M. Fidelli, B. Karadeniz, A. J. Howarth, I. Huskić, L. S. Germann, I. Halasz, M. Etter, S.-Y. Moon, R. E. Dinnebier, V. Stilinović, O. K. Farha, T. Friščić, K. Užarević, *Chem. Commun.* **2018**, *54*, 6999–7002.
[34] N. Martín, M. Dusselier, D. E. De Vos, F. G. Cirujano, *ACS Catal.* **2019**, *9*, 44–48.
[35] W. Zhou, K. Cheng, J. Kang, C. Zhou, V. Subramanian, Q. Zhang, Y. Wang, *Chem. Soc. Rev.* **2019**, *48*, 3193–3228.
[36] W. G. Cui, G. Y. Zhang, T. L. Hu, X. H. Bu, *Coord. Chem. Rev.* **2019**, *387*, 79–120.
[37] V. P. Santos, T. A. Wezendonk, J. J. Delgado-Jaén, A. Iulian-Dugulan, M. A. Nasalevich, H. U. Islam, A. Chojecki, S. Sartipi, X. Sun, A. A. Hakeem, A. C. J. Koeken, M. Ruitenbeek, T. Davidian, G. R. Meima, G. Sankar, F. Kapteijn, M. Makkee, J. Gascon, *Nat. Commun.* **2015**, *6*, 6451.
[38] X. Sun, A. I. Olivos Suarez, M. Meijerink, T. van Deelen, S. Ould-Chikh, J. Zečević, K. P. de Jong, F. Kapteijn, J. Gascon, *Nat. Commun.* **2017**, *8*, 680.
[39] M. Ronda-Lloret, S. Rico-Francés, A. Sepúlveda-Escribano, E. V. Ramos-Fernandez, *Appl. Catal. A* **2018**, *562*, 28–36.

[40] I. Luz, M. Soukri, M. Lail, *Chem. Commun.* **2018**, *54*, 8462–8465.
[41] S. I. Zones. Zeolite SSZ-13 and its method of preparation. US4544538, **1985**.
[42] E. M. Gallego, C. Li, C. Paris, N. Martín, J. Martínez-Triguero, M. Boronat, M. Moliner, A. Corma, *Chem. Eur. J.* **2018**, *24*, 14631–14635.
[43] J. Q. Chen, A. Bozzano, B. Glover, T. Fuglerud, S. Kvisle, *Catal. Today* **2005**, *106*, 103–107.
[44] M. Dusselier, M. A. Deimund, J. E. Schmidt, M. E. Davis, *ACS Catal.* **2015**, *5*, 6078–6085.
[45] Z. Li, J. Martínez-Triguero, J. Yu, A. Corma, *J. Catal.* **2015**, *329*, 379–388.
[46] M. A. Deimund, L. Harrison, J. D. Lunn, Y. Liu, A. Malek, R. Shayib, M. E. Davis, *ACS Catal.* **2016**, *6*, 542–550.
[47] Q. Zhu, J. N. Kondo, R. Ohnuma, Y. Kubota, M. Yamaguchi, T. Tatsumi, *Microporous Mesoporous Mater.* **2008**, *112*, 153–161.
[48] A. Dokania, A. Dutta Chowdhury, A. Ramirez, S. Telalovic, E. Abou-Hamad, L. Gevers, J. Ruiz-Martinez, J. Gascon, *J. Catal.* **2020**, *381*, 347–354.